# Micromechanical function of myofibrils isolated from skeletal and cardiac muscles of the zebrafish

Bogdan Iorga,[1,6] Cristian Dan Neacsu,[2] Wolfram Friedrich Neiss,[3] Raimund Wagener,[2,4] Mats Paulsson,[2,4,5] Robert Stehle,[1,4] and Gabriele Pfitzer[1,4]

[1]Institute of Vegetative Physiology, [2]Center for Biochemistry, [3]Department of Anatomy I, Faculty of Medicine, [4]Center of Molecular Medicine of Cologne, and [5]Cologne Excellence Cluster on Cellular Stress Responses in Ageing-Associated Diseases, University of Cologne, Cologne 50931, Germany

[6]Department of Physical Chemistry, Faculty of Chemistry, University of Bucharest, 030018 Bucharest, Romania

The zebrafish is a potentially important and cost-effective model for studies of development, motility, regeneration, and inherited human diseases. The object of our work was to show whether myofibrils isolated from zebrafish striated muscle represent a valid subcellular contractile model. These organelles, which determine contractile function in muscle, were used in a fast kinetic mechanical technique based on an atomic force probe and video microscopy. Mechanical variables measured included rate constants of force development ($k_{ACT}$) after $Ca^{2+}$ activation and of force decay ($\tau_{REL}{}^{-1}$) during relaxation upon $Ca^{2+}$ removal, isometric force at maximal ($F_{max}$) or partial $Ca^{2+}$ activations, and force response to an external stretch applied to the relaxed myofibril ($F_{pass}$). Myotomal myofibrils from larvae developed greater active and passive forces, and contracted and relaxed faster than skeletal myofibrils from adult zebrafish, indicating developmental changes in the contractile organelles of the myotomal muscles. Compared with murine cardiac myofibrils, measurements of adult zebrafish ventricular myofibrils show that $k_{ACT}$, $F_{max}$, $Ca^{2+}$ sensitivity of the force, and $F_{pass}$ were comparable and $\tau_{REL}{}^{-1}$ was smaller. These results suggest that cardiac myofibrils from zebrafish, like those from mice, are suitable contractile models to study cardiac function at the sarcomeric level. The results prove the practicability and usefulness of mechanical and kinetic investigations on myofibrils isolated from larval and adult zebrafish muscles. This novel approach for investigating myotomal and myocardial function in zebrafish at the subcellular level, combined with the powerful genetic manipulations that are possible in the zebrafish, will allow the investigation of the functional primary consequences of human disease–related mutations in sarcomeric proteins in the zebrafish model.

The Journal of General Physiology



## INTRODUCTION

The zebrafish (*Danio rerio*) has emerged as a valuable and cost-effective model organism for investigations of genotype–phenotype relations and has been widely used for studies of development, regeneration, and inherited human diseases. Zebrafish embryos exhibit early motility, and because they are transparent, microscopic investigations of the muscle function can be performed in vivo (Felsenfeld et al., 1990; Granato et al., 1996; Kane et al., 1996). Juvenile or adult zebrafish represent an outstanding model for the study of motility (van Leeuwen et al., 2008), muscle remodeling under different environmental conditions (Georga and Koumoundouros, 2010), and mechanisms regulating the regeneration of the fish heart after an injury (Poss, 2007).

Despite the emerging significance of the zebrafish as a model organism for the study of skeletal and cardiac muscle development and pathology (Nasevicius and Ekker, 2000; Udvadia and Linney, 2003; Huang et al., 2005; Guyon et al., 2007), only a few studies have attempted to characterize the physiological activity of zebrafish skeletal and cardiac muscles (Brette et al., 2008; Dou et al., 2008; Sun et al., 2008). In the only study regarding myotomal muscle contractility in zebrafish larvae, Dou et al. (2008) explored contractile and structural parameters of intact and permeabilized skeletal muscles using almost the whole larvae. Thus, the measured functional properties reflected the integral properties of the entire muscular body.

To understand better the developmental changes of the muscle in normal and pathological conditions, there is a need to analyze muscle function not only at the level of the whole larva but also at the level of the contractile organelles, i.e., the myofibrils that directly determine muscle contractility. The knockdown of sarcomeric proteins in larvae, for example, not only induces structural alterations inside the myotomal segments but also affects the sarcomere–membrane interaction and the overall shape of myotomes (Zhang et al., 2009).

Correspondence to Bogdan Iorga: bogdan.iorga@uni-koeln.de

Abbreviations used in this paper: CSA, cross-sectional area; dpf, days post fertilization; GLA, glutaraldehyde; SL, sarcomere length; TEM, transmission electron microscopy.



The Rockefeller University Press $30.00
J. Gen. Physiol. Vol. 137 No. 3 255–270
www.jgp.org/cgi/doi/10.1085/jgp.201010568

Mechanical investigations of isolated myofibrils allow the dissection of the direct effects on sarcomeric function from effects that may arise from altered compliance of the intersegmental boundaries between the myotomes (Henry et al., 2005). To our knowledge, there are no reports regarding the mechanical characterization of the zebrafish muscle function at the single myotomal or myofibrillar level.

Subcellular myofibrils, which preserve the entire contractile and regulatory apparatus of skinned striated muscle fibers, are small enough to avoid diffusion problems and, therefore, allow the simultaneous measurement of force kinetics and length changes of individual sarcomeres along the myofibril after rapid changes in $Ca^{2+}$ concentration (Stehle et al., 2002, 2009; Lionne et al., 2003).

To elucidate developmental changes in contractile muscle function, we determined the mechanical properties of skeletal myofibrils isolated from zebrafish larvae and adults. In addition, we measured the $Ca^{2+}$-regulated isometric force and the kinetics of force development in ventricular myofibrils from adult zebrafish. As the mouse is a well-established animal model for human cardiac diseases (Dalloz et al., 2001; Iorga et al., 2008), the functional properties of cardiac myofibrils from adult zebrafish were compared with the corresponding parameters measured in murine cardiac myofibrils. Although we have not yet succeeded in isolating cardiac myofibrils from the extremely small ventricles of the larvae, our study is the first to explore zebrafish cardiac contractile function at the sarcomere level.

Our results validate myofibrils isolated from myotomes of the zebrafish larvae and from myotomes and myocardium of the adult zebrafish as potentially important novel tools for mechanistic studies of skeletal and cardiac muscle function at the subcellular level.

## MATERIALS AND METHODS

### Preparation of zebrafish heart and skeletal muscle

Zebrafish were bred in the facilities of the Center for Biochemistry at University of Cologne. Experiments conformed to the Guide for the Care and Use of Laboratory Animals (1996. National Academy of Sciences, Washington D.C.).

12-mo-old adult zebrafish were anaesthetized for 5 min with a 1/100 dilution of a 4-mg/ml tricaine stock solution (Sigma-Aldrich). The fish were transferred to ice-cooled dissection buffer (see below) and immediately killed by removing the head. The heart was removed (Fig. 1 K), transferred to 500 µl of fresh dissection buffer, and stored on ice. The skin was completely removed to access the caudal skeletal muscles (Fig. 1 F). As many pigment cells as possible were removed during dissection to reduce interference with the later laser measurements. First, the whole tail skeletal muscle was excised with minimal mechanical damage and transferred to 500 µl of dissection buffer (see below). Then, the dorsal middle-posterior part of the muscle was dissected and further examined to gently remove as many of the accessible thick myosepta as possible, repeatedly washed in the dissection buffer to remove fat cells, and then stored on ice for the myofibril preparation.

The heads and caudal fins of 4–days post fertilization (dpf) zebrafish larvae, which exhibit short burst-like swimming behavior at this stage, were removed (Fig. 1 A) while the larvae were immersed in dissection buffer (see below). The epithelium was chemically removed (Fig. 1 B) using skinning buffer containing detergent (see below). Between 20 and 30 "demembranated tails" were used for each preparation of myofibrils.

Adult murine papillary muscles used for myofibril preparation were dissected from the hearts of 3-mo-old mice as described previously (Stehle et al., 2002).

### Experimental buffer and myofibril preparation

Skeletal muscles and hearts from zebrafish and murine papillary muscles were prepared in dissection buffer (pCa ≥ 7.5) containing 10 mM imidazole, 3 mM $Na_2ATP$, 6 mM Mg $acetate_2$, 5 mM $K_4$-$acetate_2$ EGTA (including 5 mM EGTA and 10 mM K-acetate), 47.7 mM $Na_2$ phosphocreatine, 2 mM DTT, 5 mM $NaN_3$, 30 mM BDM, and protease inhibitor cocktail (including 0.5 mM ABESF, 10 µM leupeptine, 10 µM antipain, and 5 µg/ml aprotinin), adjusted to pH 7.0 at 4°C with KOH.

The excised skeletal muscle tissue and two to three ventricles from zebrafish adults were permeabilized in separate small test tubes for ∼1 h at 0–4°C in skinning buffer obtained by adding 1% Triton X-100 (vol/vol) to the dissection buffer. Zebrafish larvae tails were permeabilized for ∼30 min, and murine papillary muscles were permeabilized for ∼2 h. After the detergent permeabilization step, muscle tissues were washed twice for ∼15 min in fresh dissection buffer and stored for up to 3 d at 0–4°C. Myofibrils were prepared just before the experiment by homogenization at ∼4°C for 4–5 s at maximum speed with a mini-blender (rotor of 5-mm diameter; Ultra-Turrax; IKA Works). Because zebrafish skeletal myofibrils are stickier than cardiac myofibrils, and because myofibrils from larval myotomes and adult hearts were prepared in smaller batches than adult zebrafish skeletal and murine cardiac myofibrils, only the homogenates of adult tissues were further filtered through a 22-µm polypropylene mesh to remove aggregated myofibrils and large bundles.

The slack sarcomere length ($SL_0$) of isolated myofibrils was measured in relaxing buffer (pCa 7.5; ionic strength, 190 mM) containing 10 mM imidazole, 1 mM $Na_2$ ATP, 6 mM Mg-$acetate_2$, 3 mM $K_4$-$acetate_2$ EGTA (including 3 mM EGTA and 6 mM K-acetate), 47.7 mM $Na_2$ phosphocreatine, and 2 mM DTT, adjusted to pH 7.0 at 10°C with KOH. The myofibrils were fully $Ca^{2+}$ activated (pCa 4.5, pH 7.0, at 10°C; ionic strength, 190 mM) using a similar buffer containing 3 mM $K_4$-$acetate_2$ CaEGTA (including 3 mM EGTA and 3 mM Ca-$acetate_2$) instead of 3 mM $K_4$-$acetate_2$ EGTA, called the $Ca^{2+}$-activating buffer. To determine the $Ca^{2+}$ sensitivity of the generated isometric force, myofibrils were exposed to $Ca^{2+}$-activating buffers with intermediate calcium concentrations, obtained by varying the ratio of CaEGTA/EGTA.

### Mechanical setup and experimental protocol

The experimental setup for the recording force transients generated by isolated myofibrils has been described (Stehle et al., 2002). In brief, 500–600 µl of myofibrillar suspension was placed on the floor of a glass chamber thermostated at 10°C. Myofibrils were allowed to sediment for ∼1 h, and then the chamber was filled with relaxing buffer. Small myofibrillar bundles of 2–9 µm in diameter and 30–80 µm in length were attached to a stiff microneedle at one end and to the tip of an atomic force cantilever (PPP-FM type; NANOSENSORS) at the other end using silicone adhesive. After mounting, the myofibrils were stretched by 15% beyond their slack lengths as previously applied to myofibrils from other species (Stehle et al., 2002; Iorga et al., 2008). To initiate activation and relaxation of the myofibrils, rapid changes (∼10 ms) in $Ca^{2+}$ concentrations were applied to the mounted myofibrils using a fast solution change technique. A protocol of

rapid mechanical–induced slackening and restretch with the magnitude of at least 15% of myofibril total length was applied to the myofibril to determine the generated isometric steady force during $Ca^{2+}$ activation and the steady passive force in relaxing buffer. Length changes of the individual sarcomeres along the myofibril were observed with an inverted microscope (IX-70; Olympus). The sarcomere length (SL) and the cross-sectional area (CSA) were determined in bright field. If not otherwise stated, all experiments were performed at 10°C.

### Electron microscopy

Dissected and chemically permeabilized heart and caudal skeletal white muscle from adult zebrafish were immobilized with multiple pins in a small box filled with the dissection buffer to maintain constant size. The bottom of the box was made of Sylgard silicone elastomer (Corning). Muscular samples were then fixed in two different conditions: relaxed and in rigor. For the "relaxed" muscular preparation, 6% (vol/vol) glutaraldehyde (GLA) was added to the dissection buffer. For the "rigor" muscular preparation, the dissection buffer was subsequently replaced by rigor buffer with a composition similar to relaxing buffer, containing 6 mM instead of 3 mM Mg-acetate$_2$, but without $K_2Na_2$-acetate$_2$ Mg-ATP. After incubation on ice for at least 1 h, 6% (vol/vol) GLA was added to the rigor buffer. Tissues were then washed in 0.1 M of sodium cacodylate buffer, pH 7.4 (Shindo et al., 1984), postfixed for 120 min with 1% (wt/vol) $OsO_4$ in the same buffer, washed again in cacodylate buffer, dehydrated with acetone, infiltrated with and embedded in araldite CY212 (Durcupan ACM; Sigma-Aldrich), and polymerized for 48 h at 70°C as described previously (Neiss, 1984). Semi-thin sections were cut with a diamond knife (DiATOME) on an Ultracut E (Reichert, Inc.) at 0.5 µm thickness, mounted on glass slides, and stained with toluidine blue. Ultrathin sections were cut at gray interference color (30–40 nm) with a low compression 35° diamond knife (DiATOME), mounted on formvar/carbon-coated 400-mesh copper grids (square pattern; 5-µm bar thickness), and contrasted with uranyl acetate and lead citrate (Neiss, 1983). Transmission electron microscopy (TEM) was performed with an electron microscope (80 kV, 500-µm condenser 1 aperture, 200-µm condenser 2 aperture, 30-µm objective aperture; EM109; Carl Zeiss, Inc.) equipped with a temperature-stabilized wide-angle side-entry CCD camera (1,024 × 1,024 pixels, 14-bit grayscale/pixel, YAC-scintillator; Troendle Restlichtverstärker-Systeme). Magnification of the TEM images was calibrated with a cross-grating replica (2,160 lines/mm; Plano GmbH).

### Data analysis

To determine the myofibrillar force kinetic parameters, force transients were fitted by either a mono-exponential function to derive $k_{ACT}$ or by a biphasic function consisting of a linear and an exponential term to derive $k_{LIN}$, $t_{LIN}$, and $k_{REL}$, as explained previously (Stehle et al., 2002, 2009). Relaxation time constant ($\tau_{REL}$) was calculated as a function of all relaxation kinetic parameters:

$$\tau_{REL} = t_{LIN} + \frac{1}{k_{REL}} + \frac{\ln(1 - k_{LIN} t_{LIN})}{k_{REL}}, \quad (1)$$

where $k_{LIN}$ is the rate constant of the first, linear phase of the slow force decay, $t_{LIN}$ is its duration, and $k_{REL}$ is the rate constant of the second, mono-exponential phase of the fast force decay initiated by the lengthening of sarcomeres (Stehle et al., 2009). The overall rate constant of the myofibrillar relaxation process was defined as $1/\tau_{REL}$.

Force–pCa relations were fitted by the sigmoidal Hill equation:

$$F(pCa) = \frac{F_{max}}{1 + 10^{n_H (pCa_{50} - pCa)}}, \quad (2)$$

where $F$ is the force at pCa = $-\mathrm{LOG}_{10}[Ca^{2+}]$, $F_{max}$ is the maximum force at pCa 4.5 recorded for the first $Ca^{2+}$ activation, p$Ca_{50}$ is the pCa at which $F$ is 50% of $F_{max}$, and $n_H$ is the steepness of the force–pCa relation (Hill coefficient).

To determine the energy of activation ($E_a$) from the slope of the temperature dependence of the rate constants, the Arrhenius equation was used in the linear form:

$$\ln k = -\frac{E_a}{R} \cdot \frac{1}{T} + \ln A, \quad (3)$$

where $k$ ($s^{-1}$) is the rate constant, $R = 8.314472$ J/mol·K, $T$ (K) is the absolute temperature, and ln$A$ is the intercept of the y axis when x = 0.

In the absence of $Ca^{2+}$, myofibrils were successively stretched to different SLs ($SL > SL_0$), and then suddenly released back to their slack lengths after a 15-s delay, allowing time for stress relaxation, and the force responses (normalized to CSA) were recorded ($F_{pass}$). Values were fitted to a nonlinear explicit equation supporting the worm-like chain model of the entropic elasticity described previously (Linke and Fernandez, 2002).

No quantitative analysis of video images (Hokawo Imaging Software 2.1; Hamamatsu Photonics) was performed, except for the estimations of SLs and diameters of relaxed or $Ca^{2+}$-activated myofibrillar bundles.

Statistical analysis was performed (Prism 4.03; GraphPad Software) by subjecting data to unpaired Student's $t$ tests. Significance was set at $P < 0.05$ (*), $P < 0.01$ (**), and $P < 0.001$ (***). If not otherwise stated, all data are given as mean ± SEM of $n$ analyzed myofibrils.

### Online supplemental material

Examples of myofibrillar contractions and relaxations are shown: myotomal myofibrils from larvae and adult zebrafish (Videos 1 and 2, respectively), and cardiac myofibrils from adult zebrafish and mouse (Videos 3 and 4, respectively). The online supplemental material is available at http://www.jgp.org/cgi/content/full/jgp.201010568/DC1.

## RESULTS

### General description of the myofibril preparations

We prepared myofibrils from the dorsal middle-posterior skeletal muscles of the zebrafish adult (Fig. 1 F), as they contain fast (white) fibers that can be separated from the superficial slow (red) and intermediate (pink) muscles (van Raamsdonk et al., 1982), and most of the power involved in swimming is contributed by the muscle in the caudal region of the fish (Rome et al., 1993). However, because of the small size of the zebrafish larvae, the entire chemically permeabilized tails (Fig. 1 B) were homogenized, and the resulting myofibrils (Fig. 1 D) were harvested and investigated (Fig. 1 E). Freshly prepared myofibrils were always used in experiments, but their sarcomeric structure was preserved even after storage for 3–4 d in dissection buffer at 0–4°C.

Myotomal myofibrils isolated from either larvae or adult zebrafish (Fig. 1, D, E, H, and I) have lengths as previously reported for mammalian skeletal myofibrils (30–100 µm) (Lionne et al., 2003), but they seem to be softer and stick together and to the atomic force cantilever

or handling tools to a greater degree than mammalian skeletal or cardiac myofibrils. The homogenate of permeabilized zebrafish larvae tails does not only contain isolated thin myofibrillar bundles but also some myotome segments consisting of thin layers of myofibrils (Fig. 1 C). Isolation of myofibrillar structures from larvae is most probably facilitated by the incompletely developed connective tissue, enabling a sufficient preparation of myofibrils for mechanical studies. Parts of larger muscle myotomes from adult zebrafish can also be observed among myofibrils if the homogenate is not filtered through a mesh (Fig. 1 G). Isolated myofibrils prepared from the skeletal muscles of zebrafish larvae (Fig. 1, D, E, and P, zfL-sk; average slack SL: $SL_0$ = 2.02 ± 0.02 µm) or adult zebrafish (Fig. 1, H, I, and P, zfA-sk; $SL_0$ = 2.03 ± 0.03 µm; cf. Squire et al., 2008, ∼2.2 µm; cf. Câmara-Pereira et al., 2009, 1.7–2.0 µm) appear identical. In phase contrast (Fig. 1, I and J), they display very thin longitudinal white bands, widely axially spread out from one sarcomere to another, in addition to the well-known transverse I bands.

Cardiac myofibrils (20–50-µm length; Fig. 1 O liter-O) isolated from the ventricles of adult zebrafish (Fig. 1 K) look similar to the myofibrils prepared from murine papillary muscles (see Videos 3 and 4) (Iorga et al., 2008). Zebrafish cardiac myofibrils often branch (Figs. 1 M and 2, D and E), as observed in cardiac myofibril bundles from mammals. The mean SL of slack and relaxed cardiac (zfA-c) myofibrils ($SL_0$ = 2.12 ± 0.04 µm) from adult zebrafish does not significantly differ from that of murine cardiac (m-c) myofibrils ($SL_0$ = 2.03 ± 0.03 µm; Fig. 1 P) (Iorga et al., 2008).

In control experiments, to confirm the preservation of the integrity of the sarcomeric elements after

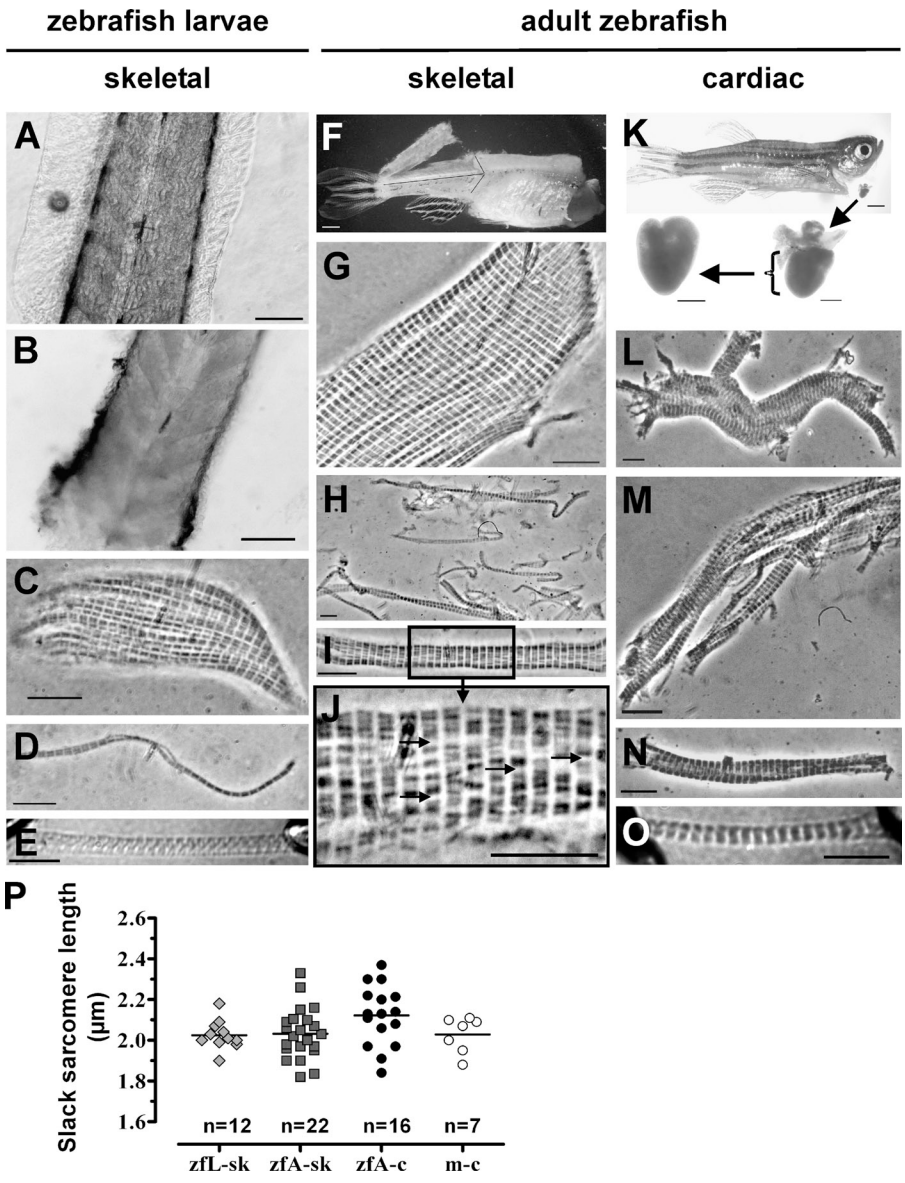


**Figure 1.** Light micrographs showing: dissected tail before (A) and after (B) detergent skinning of a 4-dpf larvae; a part of a myotome (C) and a thin myofibrillar bundle (D) isolated after homogenization of the chemically permeabilized larval tails; a myofibrillar bundle (E) isometrically mounted in the experimental setup between a stiff needle (left) and the tip of the atomic force cantilever (right) before $Ca^{2+}$ activation; skeletal muscle dissected from adult zebrafish before chemical permeabilization (F); part of a muscle myotome (G) and myofibrillar suspension (H) after homogenization of permeabilized skeletal muscles; myotomal myofibrils showing very thin longitudinal white bands, pointed to by arrows (I and magnified in J), which contain extended profiles of T-tubules and SR as shown in TEM (see Fig. 2, A–C); dissected adult zebrafish (K, top) to access the whole heart (K, bottom right) from which only ventricles (K, bottom left) were used for preparation of myofibrils; cardiac branched myofibrils (L and M) isolated from a permeabilized ventricle of the adult zebrafish; and relaxed cardiac myofibrils before (N) and after (O) mounting them isometrically in the experimental setup. Bars: C–E, G–J, and L–O, 10 µm; A and B, 100 µm; K, bottom, 500 µm; F and K, top, 2 mm. (P) Distribution of the slack SLs of relaxed (pCa 7.5) myofibrils isolated from skeletal muscles of the larvae (zfL-sk; filled diamonds), skeletal muscles of the adult zebrafish (zfA-sk; filled squares), ventricle of the adult zebrafish (zfA-c; filled circles), and papillary muscles of the murine heart (m-c; open circles). Horizontal lines indicate mean values; *n* is the number of measured myofibrils.

the permeabilization procedure using the same protocol as that used to prepare the myofibrils for the mechanical measurements, we examined the ultrastructure of the skeletal and cardiac muscles from adult zebrafish. The muscles were fixed under either rigor or relaxing conditions. Transmission electron micrographs of white skeletal (Fig. 2, A–C) and cardiac muscles (Fig. 2, D and E) revealed the known ultrastructural elements of the sarcomeres, resolving highly organized A- and I-bands with well-aligned thick and thin filaments, Z-disks, M-bands, and H-zones (Waterman, 1969; Câmara-Pereira et al., 2009; Jopling et al., 2010).

Different from other freshwater and seawater fish that contain both AI-type and Z-type triads (Akster, 1981; Suzuki et al., 2003), the white skeletal muscle of zebrafish contains only Z-type triads (Fig. 2, A–C) (Squire et al., 2008; Câmara-Pereira et al., 2009). Our electron micrographs of skeletal muscle (Fig. 2, A–C) indicate that the very thin longitudinal bands, seen at light microscopic resolution (Fig. 1, I and J; see above), are a result of the displacement and separation of myofibrils by grossly dilated T-tubules and SR (best seen in cross section: Fig. 2 A, inset). Compared with the ultrastructure of the zebrafish skeletal muscle shown in previous studies (Squire et al., 2008; Câmara-Pereira et al., 2009), in our material, the

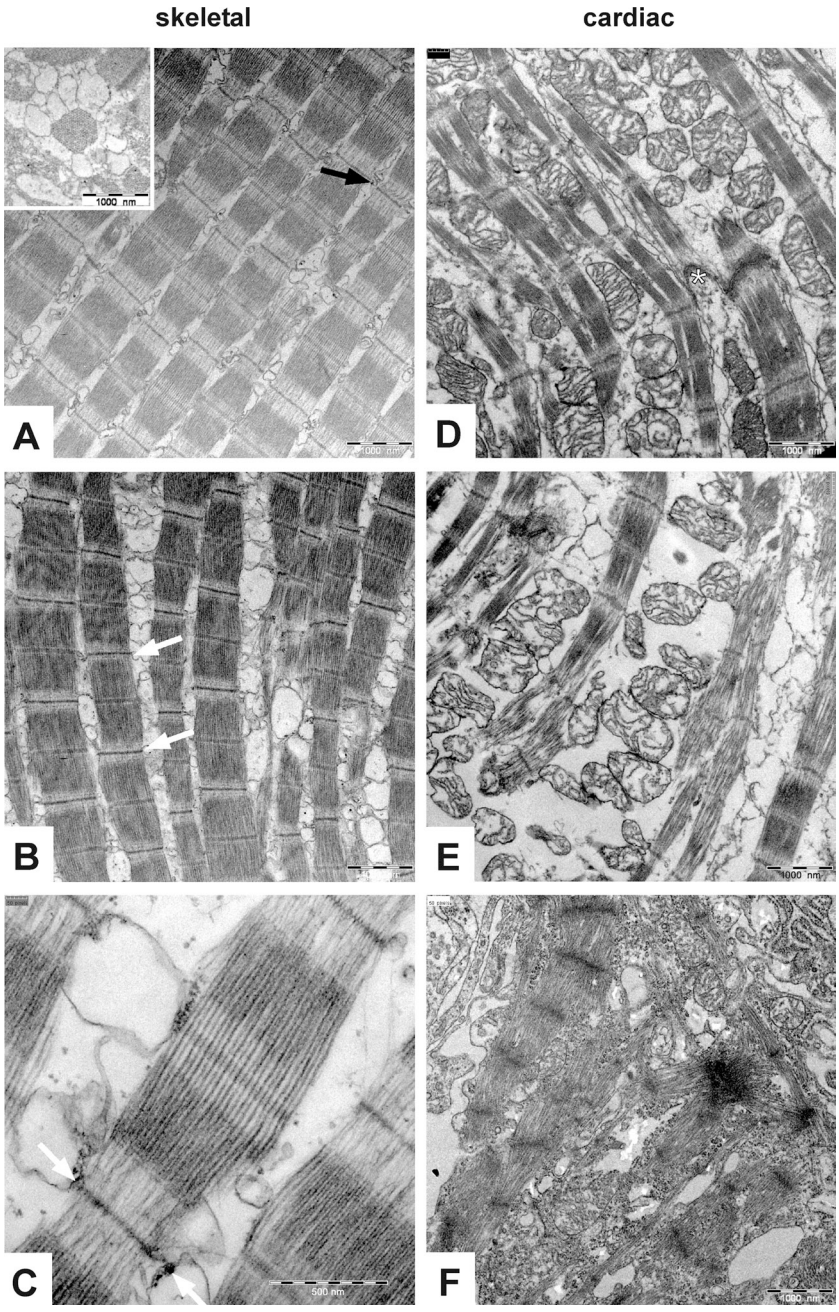


**Figure 2.** Transmission electron micrographs showing white skeletal muscle (A–C) and myocardial muscle (D and E) from adult zebrafish. Zebrafish striated muscle was prepared under relaxing (A and C) or rigor (B, D, and E) conditions before fixation. Known sarcomeric structures (thin and thick filaments; Z-disks; A-, I-, and H-bands; and M-line), SR, T-tubules only at Z-disks (arrows in A–C), and ghosts of permeabilized mitochondria (D and E) are clearly observed. The inset in A shows grossly distended profiles of SR surrounding the A-band of a myofibril in a rosetta-like arrangement in cross section. In D, an intercalated disk, specific to cardiac muscle tissue, is indicated by an asterisk, but there are no T-tubules in the myocardium. For comparison with cardiac tissue from adult zebrafish, the ultra-structure of a myocardial section from murine embryo (embryonic day 11.5) is shown in F (unpublished data). SL of the skeletal muscle from adult zebrafish is 1.8 µm in relaxing buffer (A), 1.5 µm in rigor buffer (B), and 1.6 µm in the cardiac muscle under rigor conditions (D and E). Bars: A, B, and D–F, 1.0 µm; C, 0.1 µm.

T-tubules and SR profiles were distended and the matrix of mitochondria were leached out (Fig. 2, A–C), most likely because of the membrane permeabilization before fixation.

The cardiac muscle of zebrafish lacks T-tubules (Fig. 2, D and E), "a common morphological condition in all fishes" (Di Maio and Block, 2008). In contrast to skeletal muscle, cardiac muscle sections exhibit rather thin myofibrils at low density (Fig. 2, D and E). In that respect, the myocardial ultrastructure from the ventricles of adult zebrafish resembles that usually observed in cardiac ventricles of murine embryos (Fig. 2 F; unpublished data).

In the white skeletal muscle of the zebrafish, fixed by GLA and $OsO_4$, we measured the length (mean ± SD) of thick filaments at 1.32 ± 0.06 µm ($n = 9$) and the length of thin filaments at 0.88 ± 0.05 µm ($n = 9$). These data are similar to those of fixed white skeletal muscle of the perch, a freshwater fish like the zebrafish, with 1.32-µm-long thick filaments and 0.86-µm-long thin filaments (Akster, 1981). By using the same primary fixation as ours (6% GLA), Granzier et al. (1991) measured even slightly shorter filament lengths: 1.20 µm for thick and 0.78 µm for thin filaments of perch muscle samples. However, after accounting for the shrinkage (25.6% for thick and 9.2% for thin filaments), these length values were estimated at 1.64 µm for thick filaments and 0.94 µm for thin filaments (Granzier et al., 1991). Using their correction factors for shrinkage, the length of thick and thin filaments in our zebrafish myotomal samples amounted to ∼1.77 and ∼0.97 µm, respectively. In zebrafish cardiac muscle, we measured the length of thick and thin filaments as 1.31 ± 0.11 µm ($n = 4$; or ∼1.76 µm, corrected for shrinkage) and 0.89 ± 0.06 µm (or ∼0.98 µm, corrected for shrinkage), respectively, i.e., similar to the directly measured data for zebrafish myotomal muscle. The thickness of the Z-disk amounted to 45 ± 7 nm in the zebrafish skeletal muscle and 75 ± 7 nm in the cardiac muscle. This difference is not surprising as, in general, the layers of α-actinin determine the Z-disk width: fast fibers have narrow (∼30–50-nm) Z-disks and slow and cardiac fibers have wide (∼100-nm) Z-disks (Luther, 2009).

### Steady-state and transient kinetic contractile parameters of myotomal myofibrils in zebrafish larvae and adults

We have investigated the steady-state (Fig. 4, A and B) and transient kinetic (Fig. 4, C–F) mechanical properties of the myofibrils isolated from myotomes of 4-dpf zebrafish larvae and of adult zebrafish (Table I). 4 dpf is a suitable developmental stage for studies on morphants because the morpholino-modified oligonucleotide antisense knockdown works in a transient time

TABLE I

*Steady-state and kinetic mechanical parameters measured in skeletal (larvae and adult zebrafish) and cardiac (adult zebrafish and mouse) myofibrils*

| Myofibril type: | Skeletal | | Cardiac | |
|---|---|---|---|---|
| Animal model: | Larvae zebrafish | Adult zebrafish | Adult zebrafish | Adult mouse |
| $SL_0$ (µm) | 2.02 ± 0.02 ($n = 12$) | 2.03 ± 0.03 ($n = 22$) | 2.12 ± 0.04 ($n = 16$) | 2.03 ± 0.03 ($n = 7$) |
| $F_{max}$ (nN/µm$^2$) | 40.1 ± 4.7 ($n = 11$)[a] | 18.4 ± 1.5 ($n = 22$) | 49.8 ± 4.6 ($n = 15$) | 58.1 ± 4.4 ($n = 7$) |
| $pCa_{50}$ | ND | 5.14 ± 0.02 ($n = 5$) | 5.44 ± 0.04 ($n = 8$) | 5.35 ± 0.06 ($n = 7$) |
| $n_H$ | ND | 2.38 ± 0.19 ($n = 5$) | 1.71 ± 0.23 ($n = 8$) | 1.66 ± 0.31 ($n = 7$) |
| $F_{pass}$ (nN/µm$^2$) | 4.2 ± 0.5 ($n = 10$)[a] | 2.3 ± 0.2 ($n = 22$) | 4.0 ± 0.3 ($n = 15$) | 3.3 ± 0.4 ($n = 7$) |
| $k_{ACT}$ ($s^{-1}$) | 27.0 ± 5.3 ($n = 10$)[b] | 11.3 ± 1.4 ($n = 15$) | 5.2 ± 0.6 ($n = 15$) | 5.6 ± 0.2 ($n = 7$) |
| $k_{LIN}$ ($s^{-1}$) | 11.6 ± 2.3 ($n = 11$)[c] | 6.3 ± 0.7 ($n = 10$) | 1.9 ± 0.2 ($n = 15$) | 2.2 ± 0.1 ($n = 7$) |
| $t_{LIN}$ (ms) | 16.7 ± 2.9 ($n = 11$) | 18.8 ± 2.2 ($n = 10$) | 48.7 ± 2.9 ($n = 15$)[b] | 34.6 ± 2.2 ($n = 7$) |
| $k_{REL}$ ($s^{-1}$) | 121.0 ± 22.5 ($n = 11$) | 77.1 ± 10.9 ($n = 10$) | 24.9 ± 1.5 ($n = 15$)[b] | 33.6 ± 2.3 ($n = 7$) |
| $\tau_{REL}{}^{-1}$ ($s^{-1}$) | 52.7 ± 9.9 ($n = 11$) | 34.1 ± 4.4 ($n = 10$) | 11.9 ± 0.6 ($n = 15$)[b] | 16.2 ± 1.0 ($n = 7$) |

Where applicable, values were compared between skeletal myofibrils from larvae and from adult zebrafish (second and third columns), and between cardiac myofibrils from adult zebrafish and from mouse (fourth and fifth columns). Maximum generated isometric force ($F_{max}$) was determined at saturating [$Ca^{2+}$], pCa 4.5; passive force ($F_{pass}$) was evaluated in relaxing condition (pCa 7.5) at SL = 1.15 × $SL_0$. Data for murine cardiac myofibrils was taken from (Iorga et al., 2008). ND, not determined.

[a]$P < 0.001$; unpaired $t$ test.

[b]$P < 0.01$; unpaired $t$ test.

[c]$P < 0.05$; unpaired $t$ test.

window within 1 wk after fertilization (Nasevicius and Ekker, 2000).

Isometrically mounted myofibrils, stretched by 15% beyond their slack lengths, were subjected to a rapid slack–restretch protocol (Fig. 3 A, bottom) before (pCa 7.5) and during maximal (pCa 4.5) or partial (7.5 > pCa > 4.5, only for myofibrils from adult zebrafish) $Ca^{2+}$ activation to determine the passive force response and the active force, respectively (Fig. 3 A; see Video 1 for larval myofibrils and Video 2 for myofibrils from adult zebrafish). During generation of the maximum force, sarcomeres actively shortened on average by 10.7 ± 3.1% (mean ± SD; $n = 18$) of their lengths adjusted before activation; i.e., SL during $Ca^{2+}$ activation was 2.0–2.2 µm.

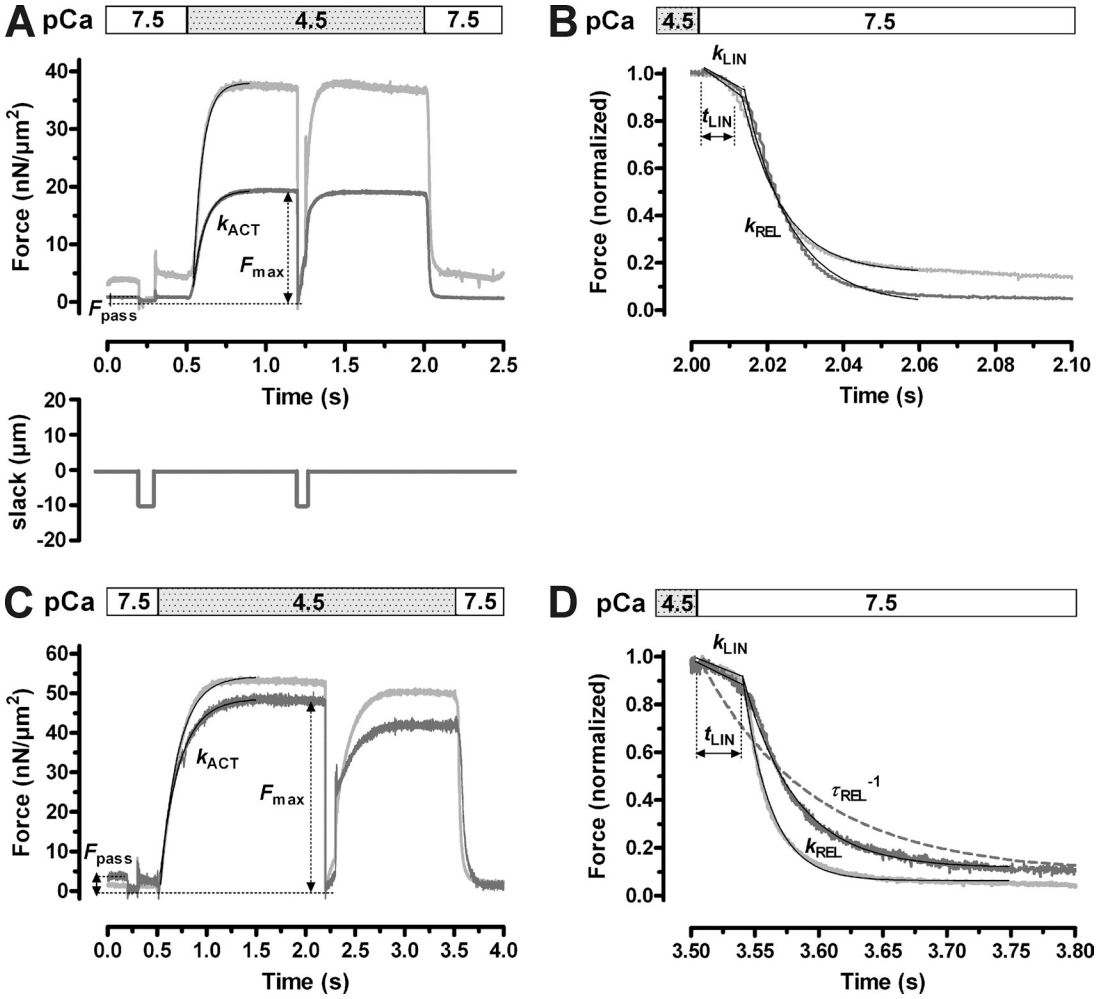


**Figure 3.** Representative force transients obtained at 10°C from isometrically mounted (as shown in Fig. 1, E and O) skeletal (A and B) and cardiac (C and D) myofibrils. (A) A full contraction–relaxation cycle of a skeletal myofibril isolated from skinned myotomes of zebrafish larvae (light gray trace; $k_{ACT}$ = 20 $s^{-1}$, $F_{max}$ = 38 nN/µm², and $F_{pass}$ = 3.4 nN/µm²; see Video 1) and adult zebrafish (dark gray trace; $k_{ACT}$ = 13 $s^{-1}$, $F_{max}$ = 20 nN/µm², and $F_{pass}$ = 1.2 nN/µm²; see Video 2). $Ca^{2+}$ concentration is rapidly (10 ms) changed from pCa 7.5 to 4.5 and back to 7.5 to induce contraction and the relaxation, respectively. Before $Ca^{2+}$ activation, the passive force ($F_{pass}$) and, during $Ca^{2+}$ activation, the maximum generated force ($F_{max}$) are determined, respectively, by transiently slackening–restretching the initially pre-stretched myofibrils at $SL = 1.15 \times SL_0$. (B) Recordings on an expanded time scale of the biphasic normalized force decay shown in A for larvae (light gray trace; $k_{LIN}$ = 10.3 $s^{-1}$, $t_{LIN}$ = 12 ms, and $k_{REL}$ = 98 $s^{-1}$) and for adult zebrafish (dark gray trace; $k_{LIN}$ = 7.6 $s^{-1}$, $t_{LIN}$ = 14 ms, and $k_{REL}$ = 79 $s^{-1}$). (C) A full contraction–relaxation cycle of a cardiac myofibril isolated from the myocardium of adult zebrafish (dark gray trace; $k_{ACT}$ = 5.2 $s^{-1}$, $F_{max}$ = 47 nN/µm² and $F_{pass}$ = 3.3 nN/µm²; see Video 3) and from murine papillary muscles (light gray trace; $k_{ACT}$ = 5.8 $s^{-1}$, $F_{max}$ = 52 nN/µm², and $F_{pass}$ = 1.8 nN/µm²; see Video 4) subjected to a protocol similar to that described for A. (D) Normalized force transients of the biphasic relaxation shown on an expanded time scale for a cardiac myofibril in C: zebrafish (dark gray trace; $k_{LIN}$ = 2.3 $s^{-1}$, $t_{LIN}$ = 46 ms, $k_{REL}$ = 25 $s^{-1}$) and mouse (light gray trace; $k_{LIN}$ = 2.1 $s^{-1}$, $t_{LIN}$ = 32 ms, and $k_{REL}$ = 42 $s^{-1}$). Dashed curve (shown only for the zebrafish cardiac myofibril) is the simulated force decay with the rate constant $1/\tau_{REL}$ calculated from kinetic parameters of the force relaxation using Eq. 1 ($\tau_{REL}^{-1}$ = 12.3 $s^{-1}$ for a zebrafish cardiac myofibril; for comparison, $\tau_{REL}^{-1}$ = 18.5 $s^{-1}$ for a murine cardiac myofibril). Mono-exponential increase (myofibril contraction) and biphasic decay comprised of a linear followed by a mono-exponential phase of decay functions were used to fit (thin black lines) force transients, yielding the kinetic parameters. Steady-state and kinetic force parameters ($F_{pass}$, $F_{max}$, $k_{ACT}$, $k_{LIN}$, $t_{LIN}$, $k_{REL}$, and $\tau_{REL}^{-1}$) are shown only for skeletal and cardiac myofibrils of the adult zebrafish.

The maximum generated isometric force ($F_{max}$, <20 nN/μm$^2$ at pCa 4.5) and the passive force ($F_{pass}$, ~2 nN/μm$^2$ at pCa 7.5) in skeletal myofibrils from adult zebrafish are smaller than $F_{max}$ (~40 nN/μm$^2$; Fig. 4 A) and $F_{pass}$ (~4 nN/μm$^2$; Fig. 4 B) recorded in skeletal myofibrils from the zebrafish larvae, respectively. Multiple $Ca^{2+}$ activations did not damage the overall observed structure of the investigated myotomal myofibrils.

The force transient (Fig. 3 A), induced by a sudden rise in [$Ca^{2+}$] from pCa 7.5 to 4.5, can be fitted by a mono-exponential function yielding the rate constant $k_{ACT}$, which estimates the kinetics of cross-bridge turnover. Upon $Ca^{2+}$ removal (from pCa 4.5 back to 7.5), the decay of force (Fig. 3 B) was biphasic, as observed in the myofibrils isolated from different mammals (Stehle et al., 2002). During the first phase, the duration of which is given by $t_{LIN}$, the force decays slowly with the rate constant $k_{LIN}$, which estimates the cross-bridge detachment rate (Poggesi et al., 2005; Stehle et al., 2009). During the second phase, sarcomeres start to lengthen, accelerating cross-bridge detachment (Poggesi et al., 2005; Stehle et al., 2009), and the force further decays faster with the rate constant $k_{REL}$ (Fig. 3 B).

Our results indicate that myotomal myofibrils from larvae develop force ($k_{ACT}$; Fig. 4 C) and relax ($k_{LIN}$; Fig. 4 D) at higher rates than myotomal myofibrils from adult zebrafish (Table I), showing that the cross-bridges cyclically attach and detach at higher rates in larval myotomes. This observation suggests that skeletal myofibrils from larvae probably contain faster myosin heavy chain and/or myosin light chain isoforms than skeletal myofibrils from adult fish. The larger scatter of data (Fig. 4, C and D) may suggest the presence of a heterogeneous population of myotomal myofibrils isolated from zebrafish larvae, which is consistent with previous immunohistochemical observations (van Raamsdonk et al., 1982). The time point at which the second relaxation phase starts, $t_{LIN}$, seems to be similar for myofibrils prepared from both larvae and adult zebrafish (Fig. 4 E and Table I). Values of the rate constant $k_{REL}$ of the accelerated force decay phase are also more scattered for larval myofibrils (Fig. 4 F and Table I).

Fig. 5 A shows the isometric force generated at different intermediate $Ca^{2+}$ concentrations by skeletal myofibrils

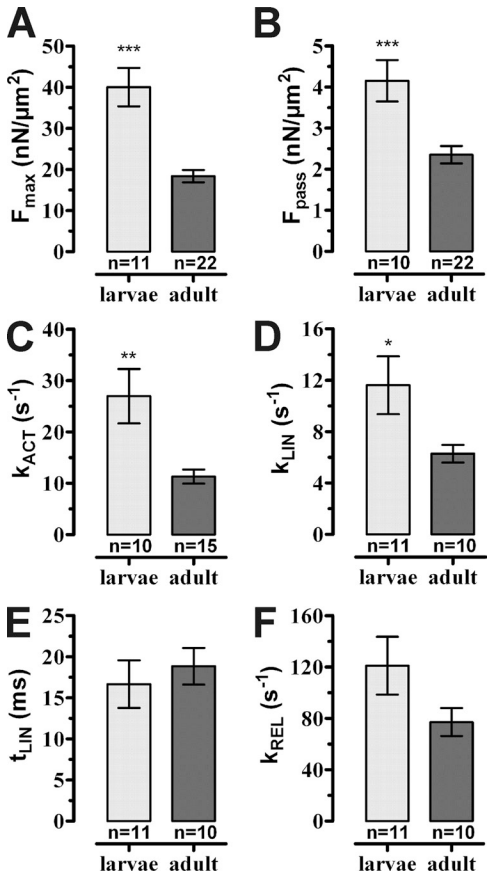


**Figure 4.** Mechanical steady-state forces. (A) $F_{max}$ determined at pCa 4.5. (B) $F_{pass}$ determined at pCa 7.5. (C–F) Kinetic parameters determined for myotomal myofibrils isolated from larvae (light-gray filled bar) and adult (dark-gray filled bar) zebrafish. (C) Rate constants of force development ($k_{ACT}$). (D–F) $k_{LIN}$, $t_{LIN}$, and $k_{REL}$ determined from relaxation time courses. *n* is the number of analyzed myofibrils at 10°C.

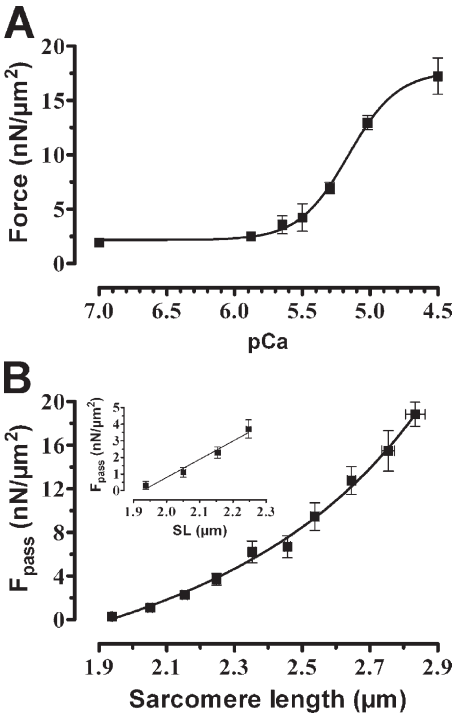


**Figure 5.** Steady-state force measured in myofibrils isolated from skeletal white muscles of the adult zebrafish determined at 10°C. (A) Force–pCa relationship of myofibrils pre-stretched 15% beyond their slack SLs; data are fitted to Eq. 2 (p$Ca_{50}$ and $n_H$ are given in Table I). (B) Passive force responses (at pCa 7.5) as a result of mechanical stretch at different successive SLs; data are fitted to the worm-like chain model of entropic elasticity. The inset shows the initial slope as an estimate of passive stiffness: 11.0 ± 1.3 kPa/μm (1 kPa = 1 nN/μm$^2$). All values were normalized to the CSA of the myofibrils.

isolated from white muscles of the adult zebrafish. $Ca^{2+}$ sensitivity of force ($pCa_{50}$) and the Hill coefficient ($n_H$) were also determined (Table I).

We used the worm-like chain model of the entropic elasticity (Linke and Fernandez, 2002) to fit the values of the passive force response from defined sarcomere elongations (Fig. 5 B) because the viscous elasticity of a fully relaxed myofibril is mainly determined by titin (Linke and Fernandez, 2002). Despite the nonlinear relationship, at small stretches under stationary mechanical conditions of the relaxed myofibril, a linear $F_{pass}$-SL dependence based on the myofibrillar elastic property was assumed. Therefore, the initial slope (Fig. 5 B, inset) can be used to estimate the passive stiffness (11.0 ± 1.3 kPa/μm; 1 kPa = 1 nN/μm$^2$) for small mechanical perturbations of the relaxed myotomal myofibrils from adult zebrafish.

### Steady-state and transient kinetic contractile parameters of cardiac myofibril in adult zebrafish

We determined the steady-state and transient kinetic mechanical properties of functional cardiac myofibrils isolated from adult zebrafish and compared them to those of murine cardiac myofibrils. Isometrically mounted cardiac myofibrils were subjected to a complete activation–relaxation cycle, as described above for myotomal myofibrils under the same experimental conditions (Fig. 3, C and D; see Video 3 for zebrafish cardiac myofibrils and Video 4 for murine cardiac myofibrils).

Maximum isometric forces generated by cardiac myofibrils isolated from the zebrafish myocardium and from murine papillary muscles are significantly greater than the maximal forces developed by skeletal myofibrils from adult fish (Table I). Multiple $Ca^{2+}$ activations did not damage the overall structure of the cardiac myofibrils studied. Fig. 6 A shows that the force–pCa relationships of cardiac myofibrils from the zebrafish and mouse look similar, although the maximum force seems slightly but not significantly elevated in murine cardiac myofibrils. This finding suggests that the $Ca^{2+}$ sensitivity of the force ($pCa_{50}$) and the Hill coefficient ($n_H$) are not very different (Table I). However, cardiac myofibrils are significantly more $Ca^{2+}$ sensitive (Fig. 6 A) than skeletal myofibrils (Fig. 5 A) from the same adult fish, and the force–pCa relation is less steep (Table I). A lower $n_H$ suggests a lesser degree of cooperativity in cross-bridge and/or $Ca^{2+}$ binding to thin filaments in cardiac than in skeletal myofibrils from adult zebrafish.

Passive force responses of cardiac myofibrils to 15% stretch above $SL_0$ (corresponding to SL of ~2.4 μm for zebrafish and to SL of ~2.3 μm for murine sarcomeres) were similar for relaxed zebrafish and murine myofibrils (Table I). In a separate experiment, at relaxing $Ca^{2+}$ concentrations, zebrafish and murine cardiac myofibrils were successively stretched from their initial $SL_0$ to different SLs (Fig. 6 B), following a similar experimental protocol and data analysis as described previously for skeletal myofibrils. The initial slopes of the $F_{pass}$–SL relationship, estimating the passive myocardial stiffness at low stretch, are similar for both zebrafish and murine myofibrils (Fig. 6 B, inset). However, upon an extensive stretch, the passive properties of zebrafish cardiac myofibrils seem to be different compared with those of murine cardiac myofibrils.

Upon $Ca^{2+}$ activation, force developed by zebrafish cardiac myofibrils raises mono-exponentially (Fig. 3 C) with the rate constant $k_{ACT}$. This rate constant is similar to the rate constant observed in murine cardiac myofibrils during the development of $Ca^{2+}$-induced force but smaller than the $k_{ACT}$ of zebrafish skeletal myofibrils (Table I).

Upon $Ca^{2+}$ removal, zebrafish cardiac myofibrils exhibit biphasic force decay in a similar way to murine cardiac myofibrils (Fig. 3 D). There is no significant difference between the rate constant $k_{LIN}$ of the slow force decay during the first phase of relaxing zebrafish cardiac myofibrils and $k_{LIN}$ corresponding to murine

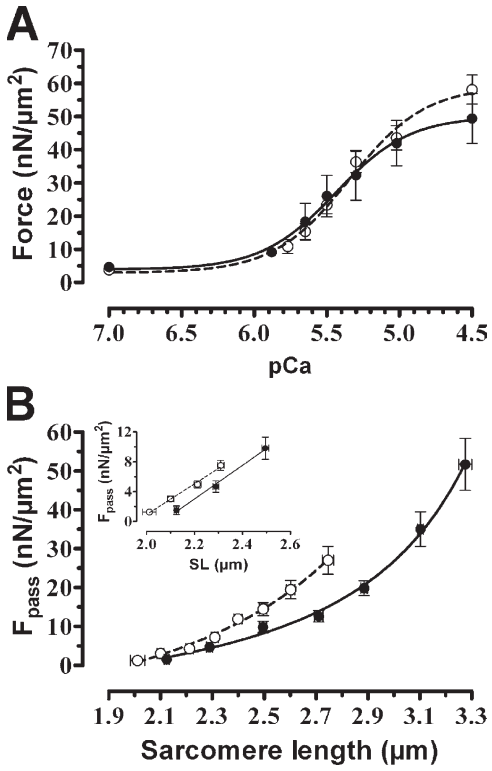


**Figure 6.** Steady-state force properties of cardiac myofibrils isolated from myocardium of adult zebrafish (filled circles) and from murine papillary muscles (open circles) determined at 10°C. (A) Force–pCa relationships from myofibrils pre-stretched by 15% beyond their slack SLs; data are fitted to Eq. 2 ($pCa_{50}$ and $n_H$ are given in Table I). (B) Passive force responses as a result of mechanical stretch at different successive SLs; data are fitted to the worm-like chain model of entropic elasticity. The inset shows the initial slopes as an estimate of the passive stiffness, 22.5 ± 1.6 kPa/μm for zebrafish and 20.5 ± 1.3 kPa/μm for mouse (1 kPa = 1 nN/μm$^2$). All values were normalized to the CSA of the myofibrils.

cardiac myofibrils (Table I). During the relaxation of the zebrafish cardiac myofibrils, after a delay $t_{LIN}$ of ~49 ms, which is significantly longer than $t_{LIN}$ determined in the murine cardiac myofibrils (~35 ms), sarcomeres start to lengthen (Video 3), accelerating cross-bridge detachment in a similar manner as observed in murine cardiac myofibrils (Video 4). These sarcomeric dynamics induces a rapid, exponential drop of the force, with the rate constant $k_{REL}$ of ~25 $s^{-1}$, which is significantly smaller than the $k_{REL}$ of murine cardiac myofibrils (Table I). As a consequence, the overall relaxation time constant, $\tau_{REL}$ (Eq. 1), is significantly larger for zebrafish cardiac myofibrils than the $\tau_{REL}$ for murine cardiac myofibrils; i.e., cardiac myofibrils isolated from the zebrafish adult relax more slowly than cardiac myofibrils isolated from mice (zebrafish $\tau_{REL}^{-1}$ < murine $\tau_{REL}^{-1}$; Table I).

It was possible to determine all kinetic parameters describing the $Ca^{2+}$ activation and relaxation processes of zebrafish cardiac myofibrils at higher temperatures (above 10°C). This allowed construction of Arrhenius plots for each of the following kinetic parameters: $k_{ACT}$, $k_{LIN}$, $t_{LIN}^{-1}$, and $k_{REL}$ (Fig. 7, A–D). Slopes from these Arrhenius plots were used to compute (Eq. 3) the energies of activation, $E_a$ (Fig. 7, A–D), which were compared with the corresponding values for murine cardiac myofibrils determined previously (Stehle et al., 2002). Corresponding to the rate constant of the force development ($k_{ACT}$), $E_a$ is smaller for zebrafish (62 kJ/mol) than for murine (72 kJ/mol) cardiac myofibrils. During the relaxation process, corresponding to $k_{LIN}$, $E_a$ is as much as 105 kJ/mol for the zebrafish cardiac myofibrils, but it was not possible to determine $E_a$ for the murine myofibrils; corresponding to $t_{LIN}^{-1}$ ($t_{LIN}$ expressed as a rate constant), $E_a$ is similar for both zebrafish (68 kJ/mol) and murine (61 kJ/mol) cardiac myofibrils; and corresponding to $k_{REL}$, $E_a$ is smaller for zebrafish (31 kJ/mol) than for murine (57 kJ/mol) cardiac myofibrils (Fig. 7, A–D).

## DISCUSSION

In this study, we explored for the first time the mechanical properties and the kinetics of force development and relaxation in myofibrils isolated from zebrafish skeletal and cardiac muscles. Electron microscopy revealed that sarcomeric ultrastructure was well preserved after our chemical permeabilization procedure. We succeeded in preparing myotomal myofibrils from early larvae. In comparison to myofibrils from adult zebrafish, larval myofibrils developed approximately twofold higher passive and active forces, and exhibited ~2.5-fold faster kinetics of $Ca^{2+}$-induced force development and slightly faster kinetics of force relaxation. Skeletal myofibrils from zebrafish, in particular those from their larvae, comprise a promising novel model for the investigation of muscle dysfunction. The cardiac myofibrils from adult zebrafish exhibited similar values of kinetic and steady-state force parameters, except for slower kinetics of force relaxation, as those of cardiac myofibrils from mice. This suggests that the myofibrils perform similarly

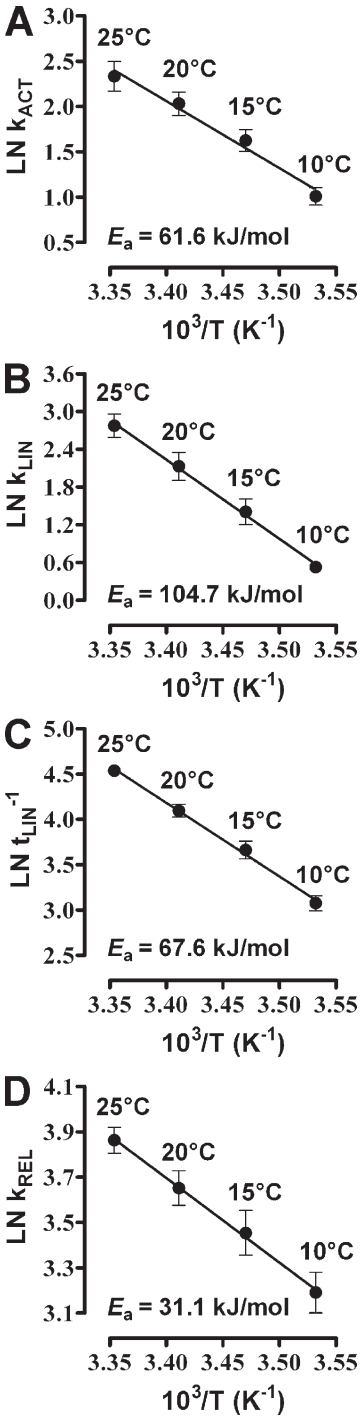


**Figure 7.** Arrhenius plots presenting the temperature dependences of the natural logarithm (LN) of kinetic parameters $k_{ACT}$ (A), $k_{LIN}$ (B), $t_{LIN}^{-1}$ (C), and $k_{REL}$ (D) for cardiac myofibrils isolated from adult zebrafish; the energies of activation ($E_a$, indicated in figures) are calculated from slopes of the linear regressions (Eq. 3) and can be compared with $E_a$ corresponding to murine cardiac myofibrils: $E_a$ = 72 kJ/mol for $k_{ACT}$, $E_a$ = 61 kJ/mol for $t_{LIN}^{-1}$, and $E_a$ = 57 kJ/mol for $k_{REL}$ (murine data taken from Stehle et al., 2002).

in the hearts of these two widely used animal models, both of which are amenable to genetic manipulation.

In the adult fish, in contrast to mammals, the fast and slow skeletal muscles are anatomically clearly separated (van Raamsdonk et al., 1982). In our study, the myotomal myofibrils were isolated from white muscles. Hence, the myofibrillar kinetic parameters should predominantly reflect the intrinsic contractile properties of the fast zebrafish skeletal muscle. However, our myofibrillar preparation from larvae at 4 dpf may not only contain myofibrils from embryonic white muscles but also myofibrils from red muscles localized at the rim of the larva (van Raamsdonk et al., 1982). For the same reason, Dou et al. (2008) assumed that there might also be a contribution of a small population of slow muscle fibers to the force response measured during sustained tetanic stimulation of the whole larvae. At present, it is not technically possible to isolate larval myofibrils only from embryonic white or red muscles for functional analysis.

### Passive force properties of zebrafish myofibrils

In skeletal myofibrils from adult zebrafish, the passive force ($F_{pass}$, ∼12.5% of $F_{max}$ at 15% stretch beyond $SL_0$; Table I) is low, whereas zebrafish larvae myofibrils exhibit higher passive force ($F_{pass}$, ∼10.5% of $F_{max}$; Table I) in response to the same stretch (Fig. 4 B). From the passive force–SL relation in the work of Dou et al. (2008), the passive stiffness of the entirety of larval muscles can be roughly estimated to be no more than 16 kPa/μm, which is comparable to that found here in myotomal myofibrils from adult zebrafish (∼11 kPa/μm; Fig. 5 B).

Because the calcification of the axial skeleton in the trunk region does not appear until 7 dpf (Du et al., 2001), during earlier larval development, the lack of stiffness provided by the skeleton might be compensated for by the existent myotomal musculature, whereas in the adult zebrafish, the axial skeleton and the dermis stiffen the body. In the adult zebrafish, myotomal fibers are distributed within the mesh of myosepta that mediates mechanical transmission of muscular force to the horizontal septa and further to the backbone and dermis, preventing lengthening of the posterior fibers when they are not yet activated. This myosepta net additionally increases the overall body stiffness. Therefore, the myosepta–myotoma system could compensate for the reduced passive stiffness of myotomal myofibrils in the adult zebrafish.

When compared with the cardiac myofibrils in the adult fish, the passive stiffness of myotomal myofibrils is about half, suggesting that myocardial tissue is stiffer than myotomal tissue. When cardiac myofibrils from zebrafish are compared with those from mice, any apparent differences in the passive force responses and stiffness are not significant if myofibrils are not extensively stretched (10°C). This is in agreement with passive force measurements only at low temperature (15°C) and reduced stretch (SL, ∼2.3 μm, similar to our case) reported for permeabilized cardiomyocytes isolated from the salmonid rainbow trout and from rats (Patrick et al., 2010). However, a larger difference in the passive force between cardiac myofibrils from zebrafish and mice seems to exist beyond ∼2.5–2.6 μm, and this could be a result of different titin isoforms and/or their distinct phosphorylation status in fish compared with mouse sarcomeres, as suggested previously (Patrick et al., 2010). Titin isoform expression in the zebrafish myotomal muscle changes at several points during early embryonic development (Steffen et al., 2007) and may also vary with the zebrafish myotomal muscle type (e.g., in white and red muscles) and with the position of the muscle along the fish (e.g., anterior, posterior), as reported for the carp (Spierts et al., 1997). The different titin isoforms might lead to different passive mechanical properties of zebrafish skeletal muscles, with the posterior being more compliant than the anterior muscles (Spierts et al., 1997). Further studies are required to clarify this aspect.

### $Ca^{2+}$-dependent active force generation of myofibrils from zebrafish cardiac muscle

The investigation of cardiac myofibrillar function was limited to the adult fish. This is because the isolation of the cardiac myofibrils for mechanical experiments from the small hearts of zebrafish larvae is a challenging task that remains to be achieved. In mammals, it is known that cardiac preparations typically develop specific forces smaller than those generated by skeletal muscles (Brutsaert and Housmans, 1977; Linke et al., 1994). Here, maximal isometric force (∼50 nN/μm$^2$) generated by adult zebrafish cardiac myofibrils is slightly lower than the force generated by cardiac myofibrils from adult mice (∼58 nN/μm$^2$), but higher than the force developed by myotomal myofibrils (<20 nN/μm$^2$).

Furthermore, we observed that the isometric force response to different $Ca^{2+}$ concentrations in zebrafish cardiac myofibrils is similar to that in murine cardiac myofibrils, i.e., similar $pCa_{50}$ and $n_H$ parameters, suggesting a comparable $Ca^{2+}$ regulation of cross-bridge cyclic interactions in cardiac sarcomeres from the adults of these two species. However, similar myofibrillar performances are surprising in view of the extremely low systolic pressure reported for the zebrafish ventricle (∼2.5 mmHg [Hu et al., 2001] compared with ∼88 mmHg for the ventricle of the adult mouse [Ishii et al., 2001]), which suggests that factors other than cross-bridges, probably external to myofibrils, account for the lower contractility of the zebrafish heart. Part of this discrepancy might be reflected by the low myofibrillar density that we observed in sections of the adult zebrafish ventricle. A similar low density of thin myofibrils is also a typical feature of the immature murine heart. During the time window of fetal development and the early

postnatal period in mice, when the heart still has a regenerative ability (Meilhac et al., 2003; Drenckhahn et al., 2008) that is similar to the heart of the adult zebrafish (Jopling et al., 2010), the systolic pressure is also low (~30 mmHg; Ishii et al., 2001). Further comparative studies could more precisely clarify the mechanisms responsible for these developmental interspecies differences.

### $Ca^{2+}$-dependent active force generation of myofibrils from zebrafish skeletal muscle

Zebrafish myotomal myofibrils generate less isometric force during the first maximal $Ca^{2+}$ activation ($F_{max}$ of ~40 nN/μm$^2$ in zebrafish larvae and $F_{max}$ of <20 nN/μm$^2$ in adult zebrafish) than do skeletal myofibrils from mammals (usually $F_{max}$, >200 nN/μm$^2$) (Edman, 2005; Poggesi et al., 2005) or from other bony fish (Altringham and Johnston, 1982). However, our values are of the same order of magnitude as those deduced from the work of Dou et al. (2008) using 5–7-dpf zebrafish larvae. Using entire larvae, they reported active forces of 35–50 nN/μm$^2$ during a twitch contraction of the intact muscle and ~10 nN/μm$^2$ for the permeabilized muscle (Dou et al., 2008). The low force of permeabilized larvae was not improved by using different muscle preparation protocols (Dou et al., 2008). p$Ca_{50}$ was lower for the permeabilized larval muscles than for the murine extensor digitorum longus muscles (Dou et al., 2008), indicating that forces generated at intermediate $Ca^{2+}$ activations are weaker in zebrafish than in murine skeletal muscles.

Possible explanations for the low isometric force are: a reduced density of the sarcomeric myofilaments, a shorter overlap region between thick and thin filaments, a different crystalline lattice of the myosin filaments, and a low cross-bridge duty ratio or weak actin–myosin interactions. A reduced number of thick and thin filaments per unit of CSA seems unlikely to explain the low force because, at least in the myotomal sarcomere of the zebrafish larvae, myofilament packing is rather more dense than in mammalian skeletal muscle (Dou et al., 2008). Shorter lengths of sarcomeric filaments can result in a smaller overlap region between myosin heads and actin filaments. However, these lengths measured from electron micrographs are likely to be underestimated values, as also reported for other fish (Herman and Dreizen, 1971; Akster, 1981), because sarcomeric filaments usually shrink with the fixing procedure (Granzier et al., 1991). In our study, all zebrafish myotomal myofibrils were stretched before $Ca^{2+}$ activation by 15% of their slack lengths (Fig. 1 P and Table I) and then shortened during maximum force development by an average of ~11% to SLs of ~2.0–2.2 μm, which are within or close to the near optimal SLs (~2.05–2.25 μm) previously determined for intact myotomal muscle of zebrafish larvae (Dou et al., 2008). Such small possible deviations from maximum generated force cannot explain the almost one order of magnitude lower force developed in zebrafish muscle when compared with the force generated by other teleosts (Altringham and Johnston, 1982) or mammals (Edman, 2005; Poggesi et al., 2005). A possible reason for lower developed force in fish myotomal muscles than in higher vertebrates was proposed previously (Squire et al., 2008): myosin filaments form a simple crystalline lattice that allows myosin heads to compete for actin-binding sites along thin filaments to a greater degree than in the super-lattice arrangement that is specific to higher vertebrate muscle. A low cross-bridge duty ratio or/and a weak actin–myosin interaction could also result in low force in muscles, as discussed separately in the next paragraph. However, we cannot rule out other, as yet unknown factors contributing to a low force of myotomal muscles from zebrafish. Therefore, further mechanistic studies are needed to provide clarifications on this matter.

### Modeling force kinetic parameters

According to Brenner's two-state cross-bridge model (Brenner, 1988), the rate constant of isometric force development represents an estimate of actin–myosin cross-bridge cycling kinetics and reflects the sum of apparent rate constants by which the cross-bridge enters and leaves the force-generating state; i.e., $k_{ACT} = f_{app} + g_{app}$. The rate constant of the initial slow relaxation phase $k_{LIN}$ is merely determined by $g_{app}$ (Poggesi et al., 2005). Estimating $g_{app}$ from $k_{LIN}$ and $f_{app}$ from $k_{ACT} - k_{LIN}$ yields values for myotomal myofibrils from larvae that are larger than those for myofibrils from adult zebrafish (Table II). This indicates faster cycling of cross-bridges in skeletal sarcomeres of larvae than in adult zebrafish, suggesting a developmental shift in myosin heavy chain isoform expression from faster larval to slower adult isoforms, which to our knowledge has not been reported. In adult zebrafish, skeletal myofibrils yield larger values for $f_{app}$ and $g_{app}$ than cardiac myofibrils, whereas the latter exhibited values similar to cardiac myofibrils from mice (Table II).

The duty ratio ($\alpha_F$), i.e., the fraction of the cycle that the cross-bridge spends in the force-generating state, can be calculated by $\alpha_F = f_{app}/(f_{app} + g_{app})$ (Brenner, 1988). The values of $\alpha_F$ are similar for larval myotomal myofibrils and cardiac myofibrils from adult zebrafish, but lower for myotomal myofibrils from adult zebrafish (Table II). This suggests that, as skeletal muscle develops from the larval to the adult stage, the duty ratio decreases.

For the definition of the isometric steady force at saturating $Ca^{2+}$ activation, $F_{max} = N \cdot \tilde{F} \cdot \alpha_F$, the product $N \cdot \tilde{F}$ can be estimated (Table II), where N is the number of cycling cross-bridges per half-sarcomere, and $\tilde{F}$ is the mean force produced by a cross-bridge in the force-generating state (Brenner, 1988). The mean value of $N \cdot \tilde{F}$ in myotomal myofibrils from larvae is significantly higher than the corresponding value in skeletal

TABLE II

*Estimated intrinsic cross-bridge parameters of skeletal (larvae and adult zebrafish) and cardiac (adult zebrafish and mouse) myofibrils based on the Brenner's model (Brenner, 1988)*

| Cross-bridges from: | Skeletal sarcomeres | | Cardiac sarcomeres | |
|---|---|---|---|---|
| | Larvae zebrafish | Adult zebrafish | Adult zebrafish | Mouse |
| $f_{app}$ ($s^{-1}$) | 16.5 ± 4.3[a] | 4.6 ± 1.1 | 3.5 ± 0.6 | 3.4 ± 0.2 |
| $g_{app}$ ($s^{-1}$) | 11.1 ± 2.2[a] | 6.3 ± 0.7 | 1.8 ± 0.1 | 2.2 ± 0.1 |
| $\alpha_F$ | 0.57 ± 0.06 | 0.40 ± 0.06 | 0.63 ± 0.04 | 0.61 ± 0.02 |
| $N \cdot \tilde{F}$ (kPa) | 71 ± 8[b] | 46 ± 4 | 79 ± 7 | 96 ± 7 |

Values were compared between skeletal myofibrils from larvae and adult zebrafish (second and third columns), and between cardiac myofibrils from adult zebrafish and mouse (fourth and fifth columns); 1 kPa = 1 nN/μm$^2$.
[a]$P < 0.05$; unpaired *t* test.
[b]$P < 0.01$; unpaired *t* test.

myofibrils from adult zebrafish (Table II). This suggests that in the larval myotomes, either the force per cross-bridge ( $\tilde{F}$ ) or the number of cycling cross-bridges (N) or both is higher than in the myotomes of the adult zebrafish. Nevertheless, it seems that apart from $N \cdot \tilde{F}$, a diminished duty ratio ($\alpha_F$) could also contribute to the lower force generated by myotomal myofibrils of the adult zebrafish.

Values of $\alpha_F$ and $N \cdot \tilde{F}$ for cardiac myofibrils from adult zebrafish and those for murine cardiac myofibrils are not significantly different (Table II), suggesting similar intrinsic kinetic and mechanical properties of cross-bridges in the hearts of the two species.

### Kinetics of force relaxation

All zebrafish myofibrils investigated here exhibited biphasic force decay transients during the relaxation process, similar to the consistent observation of two phases of force decay in myofibrils isolated from striated muscular tissues of different mammals (Stehle et al., 2002; Poggesi et al., 2005). The rate constant $k_{LIN}$ of the first phase has been proposed to estimate the intrinsic rate constant of cross-bridge detachment when thin filaments are turning off upon the rapid drop of $Ca^{2+}$ concentration, during which time sarcomeres maintain a steady length (Stehle et al., 2009; Poggesi et al., 2005). Both variables, the delay $t_{LIN}$ and the rate constant $k_{REL}$, relate to the onset and occurrence of the lengthening of the sarcomeres along the myofibril during the second phase of relaxation (see Videos 1–4). This myofibrillar structural phase of the relaxation process accelerates cross-bridge detachment, enabling the myofibril to relax (with the rate constant $k_{REL}$) faster than it contracts ($k_{REL} > k_{ACT}$) (Poggesi et al., 2005). It has been shown by chemically cross-linking cross-bridges in myofibrils (Lionne et al., 2002) that without sarcomere dynamics during the relaxation process, force continues to decay slowly with the rate constant $k_{LIN}$. As a consequence, without the structural phase of relaxation, the heart would not be able to relax sufficiently fast to enable diastolic filling and the myotomes would not be able to sustain a competent, rapid ondulatory motion of the fish.

$t_{LIN}$ and $k_{REL}$ contribute to a significantly larger relaxation time constant $\tau_{REL}$ (Eq. 1 and Table I) in zebrafish cardiac myofibrils compared with murine cardiac myofibrils. This finding assures that there is sufficient temporal resolution to investigate the relaxation transients of zebrafish cardiac myofibrils in situations where a potential intrinsic (e.g., mutation in a sarcomeric protein) or an extrinsic (e.g., higher temperature, drug targeting a sarcomeric protein) factor would accelerate relaxation kinetics. Technically, this would make the cardiac myofibril isolated from the zebrafish heart an even more attractive subcellular contractile model than the murine cardiac myofibril.

### Temperature dependence of force kinetic parameters in cardiac myofibrils

We usually investigate myofibrillar fast kinetics at low temperatures (10°C) to resolve temporally rapid force transients (Poggesi et al., 2005; Iorga et al., 2008; Stehle et al., 2009). This is also the case here with myotomal myofibrils isolated from larvae and adult zebrafish. On the contrary, cardiac myofibrils isolated from adult zebrafish contract and relax more slowly; therefore, their kinetic parameters can be determined with accuracy even at temperatures above 10°C.

Temperature dependence of the kinetics of force development can be used to predict that at the physiological temperature of the zebrafish heart ($E_a$ = 62 kJ/mol, where $E_a$ is the energy of activation), $k_{ACT}$ will be smaller than the corresponding value estimated for murine cardiac myofibrils ($E_a$ = 72 kJ/mol) at mouse body temperature (Stehle et al., 2002). $k_{LIN}$ was not determined at higher temperatures for murine cardiac myofibrils; therefore, its contribution to $\tau_{REL}$ was neglected (Eq. 1). Instead, we estimated the relaxation time constant function only of $t_{LIN}$ and $k_{REL}$: $\tau_{REL} \approx t_{LIN} + 1/k_{REL}$. Comparison of the $E_a$ of ${\tau_{REL}}^{-1}$ in zebrafish ($E_a$ = 47 kJ/mol) with its value in mice ($E_a$ = 59 kJ/mol) suggests that, at physiological temperatures (28.5°C for zebrafish and 37°C

for mice), cardiac myofibrils also relax slower in zebrafish than in mice (Stehle et al., 2002). These predictions regarding the kinetics of cardiac myofibril contraction and relaxation seem plausible because the basal heartbeat of the adult zebrafish heart (~150 bpm at 28.5°C) is slower than that of the mouse (~600 bpm at 37°C).

Overall, our findings regarding steady-state and kinetic force parameters of cardiac myofibrils support the idea that zebrafish and murine cardiac myofibrils can be considered compatible contractile models at the subcellular level.

### Potential experimental applications of myofibrils isolated from zebrafish striated muscles

The zebrafish model attracted particular interest because of the possibility of studying skeletal and cardiac muscle development (Huang et al., 2009; Sanger et al., 2009) and regeneration (Rowlerson et al., 1997; Curado et al., 2007; Poss, 2007; Jopling et al., 2010; Kikuchi et al., 2010). Despite its anatomical differences from mammalian striated muscles, the zebrafish model has been successfully applied to mimic several human muscular disease phenotypes (Zon, 1999; Shin and Fishman, 2002; Guyon et al., 2007) acquired or inherited, such as muscular dystrophies in skeletal muscles (Chambers et al., 2001; Raeker et al., 2006; Kawahara et al., 2010) or dilated or hypertrophic cardiomyopathies that compromise heart function (Dahme et al., 2009). Alteration or depletion of cardiac-specific isoforms of sarcomeric proteins in zebrafish, such as troponin C (Ohte et al., 2009; Sogah et al., 2010), troponin T (Sehnert et al., 2002), tropomyosin (Zhao et al., 2008), myosin light chain (Rottbauer et al., 2006), or titin (Seeley et al., 2007), disturbs sarcomere assembly and cardiac contractility and its regulation. Morpholino-based down-regulation of skeletal muscle protein expression in zebrafish larvae results in impaired sarcomere assembly or stability and can affect mobility (Granato et al., 1996; Raeker et al., 2006; Steffen et al., 2007). In general, the transparent zebrafish larva presents as an outstanding model for the imaging of developmentally regulated muscle-specific gene expression and the high-throughput screening of new pharmacological drugs and novel genes involved in muscle development and function. Several mutations in genes encoding for proteins of unknown function but which affect myotomal structure and animal motility or/and the morphology and contractility of the heart have been reported (Felsenfeld et al., 1990; Granato et al., 1996; Kane et al., 1996). However, the functional diagnosis in such screening studies is usually limited to the impairment of locomotion in simple touch response tests and abnormalities in the beating activity of the atrium and ventricle. Such systemic assays cannot delineate the underlying molecular basis for functional changes that could involve the neuronal system, the motor endplate, or $Ca^{2+}$ homeostasis in addition to the contractile apparatus, i.e., the myofibrils. The mechanical analysis of myofibrils isolated from zebrafish can directly test whether a dysfunction at the sarcomere level underlies the impaired motility and heart function found in such studies, because sarcomeric mechanics comprise a primary determinant of muscle function (Poggesi et al., 2005; Stehle et al., 2009). In addition, our techniques applied to zebrafish offer great potential for studying the emerging contractile function of myofibrils during sarcomerogenesis (Stainier et al., 1993; Lee et al., 1994; Hollway and Currie, 2005; Sanger et al., 2009), as well as regeneration of skeletal and cardiac muscle (Rowlerson et al., 1997; Henry et al., 2005; Jopling et al., 2010; Kikuchi et al., 2010).

### Conclusion

We have shown that myofibrils isolated from zebrafish skeletal and cardiac muscular tissues comprise a valid contractile model for functional studies of muscle, recapitulating the key features of the mammalian myofibrils. Combined with the diverse approaches and techniques available to study zebrafish to investigate organ development, function, and dysfunction, our mechanical approaches extend such functional analyses to the level of the sarcomere.

We thank Christina Schroth for technical assistance and Dr Natascha Blaudeck for advice and for supervising CS. We also thank Petra Müller for sample preparation for electron microscopy and Marco Bitzer for useful comments during manuscript writing. We are grateful to Dr. Saric and Dr. Nguemo (Institute of Neurophysiology, University of Cologne) for allowing us to show the electron micrograph of the murine fetal heart (cf. Fig. 2 F).

This work was supported by grants from the German Research Foundation (FOR1352-TP09 [STE796/3-1], SFB-612/A2, and WA1338/2-6) and the Köln-Fortune Program, Faculty of Medicine, University of Cologne.

Richard L. Moss served as editor.

Submitted: 21 October 2010
Accepted: 4 February 2011

## REFERENCES

Akster, H.A. 1981. Ultrastructure of muscle fibres in head and axial muscles of the perch (Perca fluviatilis L.). A quantitative study. *Cell Tissue Res.* 219:111–131. doi:10.1007/BF00210022

Altringham, J.D., and I.A. Johnston. 1982. The pCa-tension and force-velocity characteristics of skinned fibres isolated from fish fast and slow muscles. *J. Physiol.* 333:421–449.

Brenner, B. 1988. Effect of $Ca^{2+}$ on cross-bridge turnover kinetics in skinned single rabbit psoas fibers: implications for regulation of muscle contraction. *Proc. Natl. Acad. Sci. USA.* 85:3265–3269. doi:10.1073/pnas.85.9.3265

Brette, F., G. Luxan, C. Cros, H. Dixey, C. Wilson, and H.A. Shiels. 2008. Characterization of isolated ventricular myocytes from adult zebrafish (Danio rerio). *Biochem. Biophys. Res. Commun.* 374:143–146. doi:10.1016/j.bbrc.2008.06.109

Brutsaert, D.L., and P.R. Housmans. 1977. Load clamp analysis of maximal force potential of mammalian cardiac muscle. *J. Physiol.* 271:587–603.

Câmara-Pereira, E.S., L.M. Campos, M.A. Vannier-Santos, C.S. Mermelstein, and M.L. Costa. 2009. Distribution of cytoskeletal and adhesion proteins in adult zebrafish skeletal muscle. *Histol. Histopathol.* 24:187–196.

Chambers, S.P., A. Dodd, R. Overall, T. Sirey, L.T. Lam, G.E. Morris, and D.R. Love. 2001. Dystrophin in adult zebrafish muscle. *Biochem. Biophys. Res. Commun.* 286:478–483. doi:10.1006/bbrc.2001.5424

Curado, S., R.M. Anderson, B. Jungblut, J. Mumm, E. Schroeter, and D.Y. Stainier. 2007. Conditional targeted cell ablation in zebrafish: a new tool for regeneration studies. *Dev. Dyn.* 236:1025–1035. doi:10.1002/dvdy.21100

Dahme, T., H.A. Katus, and W. Rottbauer. 2009. Fishing for the genetic basis of cardiovascular disease. *Dis. Model. Mech.* 2:18–22. doi:10.1242/dmm.000687

Dalloz, F., H. Osinska, and J. Robbins. 2001. Manipulating the contractile apparatus: genetically defined animal models of cardiovascular disease. *J. Mol. Cell. Cardiol.* 33:9–25. doi:10.1006/jmcc.2000.1289

Di Maio, A., and B.A. Block. 2008. Ultrastructure of the sarcoplasmic reticulum in cardiac myocytes from Pacific bluefin tuna. *Cell Tissue Res.* 334:121–134. doi:10.1007/s00441-008-0669-6

Dou, Y., M. Andersson-Lendahl, and A. Arner. 2008. Structure and function of skeletal muscle in zebrafish early larvae. *J. Gen. Physiol.* 131:445–453. doi:10.1085/jgp.200809982

Drenckhahn, J.D., Q.P. Schwarz, S. Gray, A. Laskowski, H. Kiriazis, Z. Ming, R.P. Harvey, X.J. Du, D.R. Thorburn, and T.C. Cox. 2008. Compensatory growth of healthy cardiac cells in the presence of diseased cells restores tissue homeostasis during heart development. *Dev. Cell.* 15:521–533. doi:10.1016/j.devcel.2008.09.005

Du, S.J., V. Frenkel, G. Kindschi, and Y. Zohar. 2001. Visualizing normal and defective bone development in zebrafish embryos using the fluorescent chromophore calcein. *Dev. Biol.* 238:239–246. doi:10.1006/dbio.2001.0390

Edman, K.A. 2005. Contractile properties of mouse single muscle fibers, a comparison with amphibian muscle fibers. *J. Exp. Biol.* 208:1905–1913. doi:10.1242/jeb.01573

Felsenfeld, A.L., C. Walker, M. Westerfield, C. Kimmel, and G. Streisinger. 1990. Mutations affecting skeletal muscle myofibril structure in the zebrafish. *Development.* 108:443–459.

Georga, I., and G. Koumoundouros. 2010. Thermally induced plasticity of body shape in adult zebrafish Danio rerio (Hamilton, 1822). *J. Morphol.* 271:1319–1327. doi:10.1002/jmor.10874

Granato, M., F.J. van Eeden, U. Schach, T. Trowe, M. Brand, M. Furutani-Seiki, P. Haffter, M. Hammerschmidt, C.P. Heisenberg, Y.J. Jiang, et al. 1996. Genes controlling and mediating locomotion behavior of the zebrafish embryo and larva. *Development.* 123:399–413.

Granzier, H.L., H.A. Akster, and H.E. Ter Keurs. 1991. Effect of thin filament length on the force-sarcomere length relation of skeletal muscle. *Am. J. Physiol.* 260:C1060–C1070.

Guyon, J.R., L.S. Steffen, M.H. Howell, T.J. Pusack, C. Lawrence, and L.M. Kunkel. 2007. Modeling human muscle disease in zebrafish. *Biochim. Biophys. Acta.* 1772:205–215.

Henry, C.A., I.M. McNulty, W.A. Durst, S.E. Munchel, and S.L. Amacher. 2005. Interactions between muscle fibers and segment boundaries in zebrafish. *Dev. Biol.* 287:346–360. doi:10.1016/j.ydbio.2005.08.049

Herman, L., and P. Dreizen. 1971. Electron microscopic studies of skeletal and cardiac muscle of a benthic fish. I. Myofibrillar structure in resting and contracted muscle. *Am. Zool.* 11:543–557.

Hollway, G., and P. Currie. 2005. Vertebrate myotome development. *Birth Defects Res. C Embryo Today.* 75:172–179. doi:10.1002/bdrc.20046

Hu, N., H.J. Yost, and E.B. Clark. 2001. Cardiac morphology and blood pressure in the adult zebrafish. *Anat. Rec.* 264:1–12. doi:10.1002/ar.1111

Huang, C.J., T.S. Jou, Y.L. Ho, W.H. Lee, Y.T. Jeng, F.J. Hsieh, and H.J. Tsai. 2005. Conditional expression of a myocardium-specific transgene in zebrafish transgenic lines. *Dev. Dyn.* 233:1294–1303. doi:10.1002/dvdy.20485

Huang, W., R. Zhang, and X. Xu. 2009. Myofibrillogenesis in the developing zebrafish heart: a functional study of tnnt2. *Dev. Biol.* 331:237–249. doi:10.1016/j.ydbio.2009.04.039

Iorga, B., N. Blaudeck, J. Solzin, A. Neulen, I. Stehle, A.J. Lopez Davila, G. Pfitzer, and R. Stehle. 2008. Lys184 deletion in troponin I impairs relaxation kinetics and induces hypercontractility in murine cardiac myofibrils. *Cardiovasc. Res.* 77:676–686. doi:10.1093/cvr/cvm113

Ishii, T., T. Kuwaki, Y. Masuda, and Y. Fukuda. 2001. Postnatal development of blood pressure and baroreflex in mice. *Auton. Neurosci.* 94:34–41. doi:10.1016/S1566-0702(01)00339-3

Jopling, C., E. Sleep, M. Raya, M. Martí, A. Raya, and J.C. Belmonte. 2010. Zebrafish heart regeneration occurs by cardiomyocyte dedifferentiation and proliferation. *Nature.* 464:606–609. doi:10.1038/nature08899

Kane, D.A., H.M. Maischein, M. Brand, F.J. van Eeden, M. Furutani-Seiki, M. Granato, P. Haffter, M. Hammerschmidt, C.P. Heisenberg, Y.J. Jiang, et al. 1996. The zebrafish early arrest mutants. *Development.* 123:57–66.

Kawahara, G., J.R. Guyon, Y. Nakamura, and L.M. Kunkel. 2010. Zebrafish models for human FKRP muscular dystrophies. *Hum. Mol. Genet.* 19:623–633. doi:10.1093/hmg/ddp528

Kikuchi, K., J.E. Holdway, A.A. Werdich, R.M. Anderson, Y. Fang, G.F. Egnaczyk, T. Evans, C.A. Macrae, D.Y. Stainier, and K.D. Poss. 2010. Primary contribution to zebrafish heart regeneration by gata4(+) cardiomyocytes. *Nature.* 464:601–605. doi:10.1038/nature08804

Lee, R.K., D.Y. Stainier, B.M. Weinstein, and M.C. Fishman. 1994. Cardiovascular development in the zebrafish. II. Endocardial progenitors are sequestered within the heart field. *Development.* 120:3361–3366.

Linke, W.A., and J.M. Fernandez. 2002. Cardiac titin: molecular basis of elasticity and cellular contribution to elastic and viscous stiffness components in myocardium. *J. Muscle Res. Cell Motil.* 23:483–497. doi:10.1023/A:1023462507254

Linke, W.A., V.I. Popov, and G.H. Pollack. 1994. Passive and active tension in single cardiac myofibrils. *Biophys. J.* 67:782–792. doi:10.1016/S0006-3495(94)80538-7

Lionne, C., B. Iorga, R. Candau, N. Piroddi, M.R. Webb, A. Belus, F. Travers, and T. Barman. 2002. Evidence that phosphate release is the rate-limiting step on the overall ATPase of psoas myofibrils prevented from shortening by chemical cross-linking. *Biochemistry.* 41:13297–13308. doi:10.1021/bi0260278

Lionne, C., B. Iorga, R. Candau, and F. Travers. 2003. Why choose myofibrils to study muscle myosin ATPase? *J. Muscle Res. Cell Motil.* 24:139–148. doi:10.1023/A:1026045328949

Luther, P.K. 2009. The vertebrate muscle Z-disc: sarcomere anchor for structure and signalling. *J. Muscle Res. Cell Motil.* 30:171–185. doi:10.1007/s10974-009-9189-6

Meilhac, S.M., R.G. Kelly, D. Rocancourt, S. Eloy-Trinquet, J.F. Nicolas, and M.E. Buckingham. 2003. A retrospective clonal analysis of the myocardium reveals two phases of clonal growth in the developing mouse heart. *Development.* 130:3877–3889. doi:10.1242/dev.00580

Nasevicius, A., and S.C. Ekker. 2000. Effective targeted gene 'knockdown' in zebrafish. *Nat. Genet.* 26:216–220. doi:10.1038/79951

Neiss, W.F. 1983. Extraction of osmium-containing lipids by section staining for TEM. *Histochemistry.* 79:245–250. doi:10.1007/BF00489786

Neiss, W.F. 1984. Electron staining of the cell surface coat by osmium-low ferrocyanide. *Histochemistry.* 80:231–242. doi:10.1007/BF00495771

Ohte, N., I. Miyoshi, D.C. Sane, and W.C. Little. 2009. Zebrafish with antisense-knockdown of cardiac troponin C as a model of hereditary dilated cardiomyopathy. *Circ. J.* 73:1595–1596. doi:10.1253/circj.CJ-09-0523

Patrick, S.M., A.C. Hoskins, J.C. Kentish, E. White, H.A. Shiels, and O. Cazorla. 2010. Enhanced length-dependent $Ca^{2+}$ activation in fish cardiomyocytes permits a large operating range of sarcomere lengths. *J. Mol. Cell. Cardiol.* 48:917–924. doi:10.1016/j.yjmcc.2010.02.008

Poggesi, C., C. Tesi, and R. Stehle. 2005. Sarcomeric determinants of striated muscle relaxation kinetics. *Pflugers Arch.* 449:505–517. doi:10.1007/s00424-004-1363-5

Poss, K.D. 2007. Getting to the heart of regeneration in zebrafish. *Semin. Cell Dev. Biol.* 18:36–45. doi:10.1016/j.semcdb.2006.11.009

Raeker, M.O., F. Su, S.B. Geisler, A.B. Borisov, A. Kontrogianni-Konstantopoulos, S.E. Lyons, and M.W. Russell. 2006. Obscurin is required for the lateral alignment of striated myofibrils in zebrafish. *Dev. Dyn.* 235:2018–2029. doi:10.1002/dvdy.20812

Rome, L.C., D. Swank, and D. Corda. 1993. How fish power swimming. *Science.* 261:340–343. doi:10.1126/science.8332898

Rottbauer, W., G. Wessels, T. Dahme, S. Just, N. Trano, D. Hassel, C.G. Burns, H.A. Katus, and M.C. Fishman. 2006. Cardiac myosin light chain-2: a novel essential component of thick-myofilament assembly and contractility of the heart. *Circ. Res.* 99:323–331. doi:10.1161/01.RES.0000234807.16034.fe

Rowlerson, A., G. Radaelli, F. Mascarello, and A. Veggetti. 1997. Regeneration of skeletal muscle in two teleost fish: Sparus aurata and Brachydanio rerio. *Cell Tissue Res.* 289:311–322. doi:10.1007/s004410050878

Sanger, J.W., J. Wang, B. Holloway, A. Du, and J.M. Sanger. 2009. Myofibrillogenesis in skeletal muscle cells in zebrafish. *Cell Motil. Cytoskeleton.* 66:556–566. doi:10.1002/cm.20365

Seeley, M., W. Huang, Z. Chen, W.O. Wolff, X. Lin, and X. Xu. 2007. Depletion of zebrafish titin reduces cardiac contractility by disrupting the assembly of Z-discs and A-bands. *Circ. Res.* 100:238–245. doi:10.1161/01.RES.0000255758.69821.b5

Sehnert, A.J., A. Huq, B.M. Weinstein, C. Walker, M. Fishman, and D.Y. Stainier. 2002. Cardiac troponin T is essential in sarcomere assembly and cardiac contractility. *Nat. Genet.* 31:106–110. doi:10.1038/ng875

Shin, J.T., and M.C. Fishman. 2002. From zebrafish to human: modular medical models. *Annu. Rev. Genomics Hum. Genet.* 3:311–340. doi:10.1146/annurev.genom.3.031402.131506

Shindo, K., T. Tsuchiya, and J.J. Matsumoto. 1984. Preparation of electron microscopy specimens of fish muscle. *Bulletin of the Japanese Society of Scientific Fisheries.* 50:1005–1008.

Sogah, V.M., F.C. Serluca, M.C. Fishman, D.L. Yelon, C.A. Macrae, and J.D. Mably. 2010. Distinct troponin C isoform requirements in cardiac and skeletal muscle. *Dev. Dyn.* 239:3115–3123. doi:10.1002/dvdy.22445

Spierts, I.L., H.A. Akster, and H.L. Granzier. 1997. Expression of titin isoforms in red and white muscle fibres of carp (Cyprinus carpio L.) exposed to different sarcomere strains during swimming. *J. Comp. Physiol. B.* 167:543–551. doi:10.1007/s003600050107

Squire, J.M., C. Knupp, and P.K. Luther. 2008. Zebrafish—topical, transparent, and tractable for ultrastructural studies. *J. Gen. Physiol.* 131:439–443. doi:10.1085/jgp.200810015

Stainier, D.Y., R.K. Lee, and M.C. Fishman. 1993. Cardiovascular development in the zebrafish. I. Myocardial fate map and heart tube formation. *Development.* 119:31–40.

Steffen, L.S., J.R. Guyon, E.D. Vogel, M.H. Howell, Y. Zhou, G.J. Weber, L.I. Zon, and L.M. Kunkel. 2007. The zebrafish runzel muscular dystrophy is linked to the titin gene. *Dev. Biol.* 309:180–192. doi:10.1016/j.ydbio.2007.06.015

Stehle, R., M. Krüger, P. Scherer, K. Brixius, R.H. Schwinger, and G. Pfitzer. 2002. Isometric force kinetics upon rapid activation and relaxation of mouse, guinea pig and human heart muscle studied on the subcellular myofibrillar level. *Basic Res. Cardiol.* 97:I127–I135. doi:10.1007/s003950200041

Stehle, R., J. Solzin, B. Iorga, and C. Poggesi. 2009. Insights into the kinetics of $Ca^{2+}$-regulated contraction and relaxation from myofibril studies. *Pflugers Arch.* 458:337–357. doi:10.1007/s00424-008-0630-2

Sun, L., C.L. Lien, X. Xu, and K.K. Shung. 2008. In vivo cardiac imaging of adult zebrafish using high frequency ultrasound (45-75 MHz). *Ultrasound Med. Biol.* 34:31–39. doi:10.1016/j.ultrasmedbio.2007.07.002

Suzuki, S., H. Nagayoshi, K. Ishino, N. Hino, and H. Sugi. 2003. Ultrastructural organization of the transverse tubules and the sarcoplasmic reticulum in a fish sound-producing muscle. *J. Electron Microsc. (Tokyo).* 52:337–347. doi:10.1093/jmicro/52.3.337

Udvadia, A.J., and E. Linney. 2003. Windows into development: historic, current, and future perspectives on transgenic zebrafish. *Dev. Biol.* 256:1–17. doi:10.1016/S0012-1606(02)00083-0

van Leeuwen, J.L., T. van der Meulen, H. Schipper, and S. Kranenbarg. 2008. A functional analysis of myotomal muscle-fibre reorientation in developing zebrafish Danio rerio. *J. Exp. Biol.* 211:1289–1304. doi:10.1242/jeb.012336

van Raamsdonk, W., L. van't Veer, K. Veeken, C. Heyting, and C.W. Pool. 1982. Differentiation of muscle fiber types in the teleost Brachydanio rerio, the zebrafish. Posthatching development. *Anat. Embryol. (Berl.).* 164:51–62. doi:10.1007/BF00301878

Waterman, R.E. 1969. Development of the lateral musculature in the teleost, Brachydanio rerio: a fine structural study. *Am. J. Anat.* 125:457–493. doi:10.1002/aja.1001250406

Zhang, R., J. Yang, J. Zhu, and X. Xu. 2009. Depletion of zebrafish Tcap leads to muscular dystrophy via disrupting sarcomere-membrane interaction, not sarcomere assembly. *Hum. Mol. Genet.* 18:4130–4140. doi:10.1093/hmg/ddp362

Zhao, L., X. Zhao, T. Tian, Q. Lu, N. Skrbo-Larssen, D. Wu, Z. Kuang, X. Zheng, Y. Han, S. Yang, et al. 2008. Heart-specific isoform of tropomyosin4 is essential for heartbeat in zebrafish embryos. *Cardiovasc. Res.* 80:200–208. doi:10.1093/cvr/cvn177

Zon, L.I. 1999. Zebrafish: a new model for human disease. *Genome Res.* 9:99–100.